



**HAL**  
open science

## Short- and long-term oxidation behaviour of an advanced Ti<sub>2</sub>AlNb alloy

M. Dadé, Vladimir A. Esin, L. Nazé, P. Sallot

► **To cite this version:**

M. Dadé, Vladimir A. Esin, L. Nazé, P. Sallot. Short- and long-term oxidation behaviour of an advanced Ti<sub>2</sub>AlNb alloy. *Corrosion Science*, 2019, 148, pp.379-387. 10.1016/j.corsci.2018.11.036 . hal-02058621

**HAL Id: hal-02058621**

**<https://hal.science/hal-02058621>**

Submitted on 21 Oct 2021

**HAL** is a multi-disciplinary open access archive for the deposit and dissemination of scientific research documents, whether they are published or not. The documents may come from teaching and research institutions in France or abroad, or from public or private research centers.

L'archive ouverte pluridisciplinaire **HAL**, est destinée au dépôt et à la diffusion de documents scientifiques de niveau recherche, publiés ou non, émanant des établissements d'enseignement et de recherche français ou étrangers, des laboratoires publics ou privés.



Distributed under a Creative Commons Attribution - NonCommercial 4.0 International License

## Short- and long-term oxidation behaviour of an advanced Ti<sub>2</sub>AlNb alloy

M. Dadé<sup>a\*</sup>, V.A. Esin<sup>a\*\*</sup>, L. Nazé<sup>a</sup>, P. Sallot<sup>b</sup>

<sup>a</sup> MINES ParisTech, PSL Research University, Centre Des Matériaux (UMR-CNRS 7633), BP 87, 91003 Evry Cedex, France

<sup>b</sup> Safran Tech, Rue des Jeunes Bois, 78772 Magny-les-Hameaux, France

\* Corresponding author

\*\* Corresponding author

E-mail addresses: [mickael.dade@mines-paristech.fr](mailto:mickael.dade@mines-paristech.fr) (M. Dadé), [vladimir.esin@mines-paristech.fr](mailto:vladimir.esin@mines-paristech.fr) (V.A. Esin)

---

### ABSTRACT

The oxidation behaviour of an advanced Ti<sub>2</sub>AlNb alloy was investigated over a temperature range of 650-800 °C in lab air for short- and long-term experiments. The mass gain increased with time and temperature and oxidation kinetics was parabolic at 650 and 700 °C for durations up to 1000 hours, while the parabolic oxidation rate was changed at 800°C between 500 and 1000 hours. Long-term oxidation experiments revealed oxide scales composed of alternating TiO<sub>2</sub> and AlNbO<sub>4</sub> layers. Results showed an improvement of the oxidation behaviour of the present alloy as compared to other titanium base alloys, including TiAlNb alloys.

*Keywords:* Ti<sub>2</sub>AlNb alloy; oxidation; microstructure;  $\alpha$ -case; diffusion

---

### 1. INTRODUCTION

Due to their good properties at high temperatures and their low density, some categories of titanium alloys - more particularly Ti-Al base alloys - are attractive candidates for intermediate temperature aerospace applications [1-3]. Ti-Al base alloys are promising materials to reduce the weight of aircraft engines, however their oxidation resistance limits the maximum service temperature (actually around 600 °C) [1,4-6]. Interactions with oxygen containing environment at high temperature not only generate a protective oxide scale by inward oxygen diffusion but also cause embrittlement of the titanium alloy due to the formation of a subsurface  $\alpha$ -case layer known to be harder than the base alloy [2].

According to Wagner's model [7], the minimum Al content required to form a protective alumina ( $\alpha$ -Al<sub>2</sub>O<sub>3</sub>) scale on the surface of Ti-Al alloys is about 59 at. % [8]. Below this concentration, a simultaneous formation of rutile (TiO<sub>2</sub>) and alumina layers is observed [8].

Compared to the conventional Ti-Al alloys, Nb containing Ti-Al alloys (including Ti<sub>2</sub>AlNb alloys) exhibit a better mechanical behaviour at high temperature [9-11] due to the presence of orthorhombic O-Ti<sub>2</sub>AlNb phase [12] together with hexagonal  $\alpha_2$  (based on hexagonal D0<sub>19</sub> Ti<sub>3</sub>Al phase) and cubic  $\beta$  phases, already present in intermediate temperature Ti-Al alloys. This orthorhombic phase is generally more simply named "O-phase" has a crystallographic structure which can be deduced from that of  $\alpha_2$ -Ti<sub>3</sub>Al phase by a slight shearing of the crystallographic lattice and ordering of the Ti and Nb atoms. Furthermore, Nb addition is known to bring a beneficial effect on the oxidation resistance [8,13] by inhibiting the oxygen diffusion, and thus reducing rutile growth rate. The Nb addition increases as well the thermodynamic activity of Al and promotes the formation of a TiN layer at the oxide/alloy interface [8]. However, a high Nb content (more than 15 at. %) results in the degradation of the oxidation resistance [13] with the formation of Nb-oxides (AlNbO<sub>4</sub> and/or Nb<sub>2</sub>O<sub>5</sub>) [14] or ordered intermetallic phases (Nb<sub>2</sub>Al) [8,15].

To improve the oxidation resistance, several protective coatings containing the O-phase were proposed [16,17]. However, those coatings cannot be used during thermal cycling due to their weak adherence. Another possibility to increase the oxidation resistance of Ti<sub>2</sub>AlNb alloys relies on an optimization of chemical composition. Several elements like Zr, Mo, Si or W were shown to be beneficial for improved oxidation resistance [10,18-21]. However, most of these oxidation experiments were carried out for exposure times shorter than 500 h, and thus the long-term oxidation resistance of Ti<sub>2</sub>AlNb alloys remains not well documented. Moreover, the influence of different alloying elements (Zr, Si and Mo) was studied separately while a conjugated beneficial effect can be expected, giving new possibilities for improving the oxidation resistance of Ti<sub>2</sub>AlNb alloys.

Therefore, the present study aims to investigate the long-term oxidation behaviour of advanced Ti<sub>2</sub>AlNb alloy containing O-phase. Short-term experiments are carried out for the comparison. The influence of cumulative alloying by Mo, Si and Zr on the oxidation resistance will be discussed in comparison with literature data of several titanium alloys currently used for compressor part of aircraft engine (Ti-64, Ti-6242 or IMI 834) and other Ti<sub>2</sub>AlNb.

## 2. MATERIAL AND METHODS

The advanced Ti<sub>2</sub>AlNb alloy (composition is given in Table 1) [22] studied in the present work was produced by vacuum arc remelting (VAR) by GfE (Germany). Then, the hot extrusion was carried out by CEFIVAL (France) on the as-cast ingot in the temperature range corresponding to the  $\beta$  phase domain. A billet cut from the extruded rod was forged in two steps in the two-phase  $\alpha_2+\beta$  temperature domain. Finally, a three-stage heat treatment was performed to obtain the final microstructure: (i) the solutionizing between 950 and 1050 °C, (ii) formation of the large primary O-phase lath-shape precipitates between 800 and 950 °C and (iii) formation of a secondary population of much smaller O-phase laths precipitates. The final microstructure obtained after these different processing steps is shown in Fig. 1. One can see the presence of  $\alpha_2$  phase, O-phase and the  $\beta$  (or B2) phase, which is in agreement with the observations done in [23].

**Table 1.** Chemical composition (at.%) of the studied alloy.

Ti	Al	Nb	Mo	Zr	Si
Bal.	23-24	21-22	1.5-2	1-1.5	0.2-0.3

Different experiments were carried out to study the oxidation behaviour of this alloy. Interrupted isothermal oxidation treatments in lab air at 650, 700 and 800 °C were performed for thermogravimetric measurements and corresponding mass gain curves. Long-term oxidation behaviour was studied at 700 °C for 2000 and 5000 hours and additional experiment was done at 800 °C for 1506 hours.

Post-oxidation characterizations were carried out using scanning electron microscopy (SEM) with a FEI Nova NanoSEM 450 operating at 15 kV fitted with an electron dispersive X-ray spectrometer (EDS). Composition analyses were conducted using an electron probe micro analysis (EPMA) with a CAMECA SX 100 operating at 15 kV and a beam current of 40 nA. Phase analysis was performed using X-Ray diffraction (XRD) with the Cu-K $\alpha$  radiation. Vickers microhardness profiles (with a load of 5 g for 10 seconds) were conducted on sample cross section for surface hardening investigation.

## 3. RESULTS

### 3.1. Global oxidation kinetics

The mass gain as a function of oxidation time in lab air measured at 650, 700 and 800 °C is shown in Fig. 2a: the mass gain increases with the temperature and oxidation time. It will be further showed that the increase in mass during oxidation is not only related to the oxide formation but also to oxygen and nitrogen surface enrichment.

The evolution of mass gain with oxidation time is usually described by a general power-law equation [24]

$$(\Delta m)^n = k_p \times t \quad (1)$$

where  $\Delta m$  is the mass gain per unit area ( $\text{mg}\cdot\text{cm}^{-2}$ ),  $k_p$  is the oxidation rate constant ( $\text{mg}^n\cdot\text{cm}^{-2n}\cdot\text{h}^{-1}$ ),  $n$  is the rate exponent and  $t$  is the oxidation time (hours).

According to Wagner's theory [7], when the oxide scale growth is controlled by diffusion, the  $n$  exponent is 2, and  $k_p$  becomes the parabolic rate constant. Excellent linearization of the square of the mass gain versus time for all experimental temperatures shown in Fig. 2b indicates that the oxidation kinetics of the studied alloy is parabolic up to 1000 hours, except that at 800 °C for which oxidation kinetics changes for exposure times greater than 500 hours.

Table 2 gives the  $k_p$  values thus identified in the parabolic rate range.

**Table 2.** Estimated values of the parabolic constant  $k_p$  for different temperatures.

Temperature (°C)	650	700	800
$k_p$ ( $\text{mg}^2\cdot\text{cm}^{-4}\cdot\text{h}^{-1}$ )	$4.2\cdot 10^{-4}$	$1.6\cdot 10^{-3}$	$8.2\cdot 10^{-3*}$

(\* valid up to 500 h of exposure)

### 3.2. Long-term oxidation at 700 °C

First, the microstructure of specimens was observed by SEM after isothermal long-term oxidation (2000 and 5000 hours) at 700 °C in air. Backscattered electron (BSE) imaging (Fig. 3) shows that both oxidation durations lead to the multi-layered oxide formation observed earlier for other titanium base alloys [14,16].

#### 3.2.1. Oxide layer

Some micro-cracks, parallel to the sample surface and probably caused by the metallographic preparation of the specimen for SEM observations, can be observed in the oxide layer (Fig. 3). The formation of these cracks should also be related to the relaxation of internal stress generated during the oxide scale growth [14,16]. The thickness of oxide layer increases with oxidation time at 700 °C from about 9  $\mu\text{m}$  for 2000 hours to 15  $\mu\text{m}$  after 5000 hours. No spallation was observed for both samples.

Figs. 4 and 5 show EPMA element maps of the specimens after oxidation at 700 °C for respectively 2000 and 5000 hours. The oxide layers formed at 700 °C are enriched by niobium, aluminium and titanium. To identify the nature of these oxides, X-ray diffraction experiments were carried out. Rutile ( $\text{TiO}_2$ ) and aluminium niobate ( $\text{AlNbO}_4$ ) are the only oxides, which could be clearly detected (Fig. 6). Increasing the oxidation time from 2000 to 5000 hours led as well to the appearance of a thin N-rich layer between the oxide and the  $\alpha$ -case layer (Figs. 4 and 5). This layer should mostly contain titanium or niobium nitrides, according to the Refs. [11,25]. However, it was not possible to identify precisely the nature of the phases in the N-rich layer in the present work.

#### 3.2.2. $\alpha$ -case layer

Oxygen EPMA maps obtained for both oxidation times (2000 and 5000 hours) at 700 °C (Figs. 4 and 5) show that the alloy underneath the oxide is enriched in oxygen and corresponds to  $\alpha$ -case layer. The thickness of the  $\alpha$ -case layer (i.e. the depth of oxygen penetration) was measured using oxygen concentration profiles obtained by EDS (Figs. 7a and c). The oxygen concentration gradually decreases from the oxide/alloy interface to the base alloy. The region where the oxygen concentration is higher than that in the base alloy corresponds to the  $\alpha$ -case layer. Moreover, oxygen enrichment is known to increase the hardness of titanium alloys. Therefore, that effect of oxygen enrichment can also be used to measure the thickness of the  $\alpha$ -case layer. The hardness was effectively found to decrease from the oxide/alloy interface and reach a constant value corresponding to the base alloy (Figs. 7b and d).

The  $\alpha$ -case thickness measured by both methods is given in Table 3. It is worth noting that results obtained by both methods are in good agreement.

**Table 3** Thickness of the  $\alpha$ -case layer ( $\mu\text{m}$ ) obtained using oxygen concentration profile (EDS) and microhardness measurements after different long-term oxidation experiments at 700 and 800 °C

Temperature (°C)	Oxidation time (hours)	EDS	Microhardness
700	2000	$53 \pm 3$	$59 \pm 5$
	5000	$73 \pm 3$	$78 \pm 5$
800	1506	$80 \pm 3$	$85 \pm 5$

### 3.3. Long-term oxidation at 800 °C

The microstructure close to oxide/alloy interface after oxidation at 800 °C for 1506 hours is shown in Fig. 8. Due to oxide spallation observed after oxidation experiment, the thickness of the oxide layer could not be measured precisely.

EPMA maps (Fig. 9) show that the oxide layer has once again a multilayer structure with alternating Ti-rich and Al-Nb-rich layers. The XRD analysis has been carried out on powder of oxide after spallation (Fig. 10). According to the results of Rietveld refinement, these layers should be composed of  $\text{TiO}_2$  and  $\text{AlNbO}_4$  with weight fractions of respectively 81 and 19 %. A N-rich layer, which was previously observed for the two samples oxidized at 700 °C, can be noticed as well on the EPMA map, close to the oxide/alloy interface after oxidation at 800 °C for 1506 hours (Fig. 9).

Similarly to the 700 °C oxidation tests, the alloy enrichment by oxygen close to oxide/alloy interface was also observed in the EPMA map (Fig. 9). Oxygen concentration profiles and microhardness measurements were used to estimate the thickness of the  $\alpha$ -case layer (Fig. 11). The values of this thickness vary from 80 to 85  $\mu\text{m}$  depending on the method (Table 3).

## 4. DISCUSSION

### 4.1. Effect of simultaneous additions of Nb, Zr and Si on the oxidation resistance

In order to analyse the effect of Nb, Zr and Si on the oxidation resistance of the present Ti<sub>2</sub>AlNb alloy, the results obtained in this study are compared with the literature data.  $k_p$  values obtained are lower than those measured for conventional  $\alpha+\beta$  titanium alloys such as Ti-6242 ( $5.1 \cdot 10^{-3} \text{ mg}^2 \cdot \text{cm}^{-4} \cdot \text{h}^{-1}$ ) [26] and IMI 834 ( $1.8 \cdot 10^{-3} \text{ mg}^2 \cdot \text{cm}^{-4} \cdot \text{h}^{-1}$ ) [27] at 700 °C, suggesting a better oxidation resistance of the studied alloy. Compared to other titanium alloys [14], the temperature dependence of

the parabolic rate constant is close to that of the Ti-22Al-25Nb alloy investigated by Leyens [14] with smaller values for the present alloy (Fig. 12).

The oxidation kinetics of the present Ti<sub>2</sub>AlNb alloy remains parabolic at 650 and 700 °C for oxidation times up to 1000 h. On the contrary, Ti-64 alloy presents a parabolic kinetic oxidation up to 650 °C that changes to linear kinetics above 650 °C [28]. Similar conclusions are drawn from oxidation results obtained for Ti-6242 alloy [26]. These results support the statement that Nb addition is beneficial for the oxidation resistance of Ti-base alloys [8,13].

As proved by Shida [18], addition of chemical elements such as Mo and Si improve the oxidation resistance of Ti-Al and Ti-Al-Nb alloys. Unlike Ti-22.6Al-25Nb-1Mo-0.25Si (at. %) alloy studied at 650 and 800 °C in Ref. [15], the oxidation kinetics of the present alloy (Ti-(23-24)Al-(21-22)Nb-(1.5-2)Mo-(1-1.5)Zr-(0.2-0.3)Si at.%) follows a parabolic law from 650 to 800 °C up to 500 hours and not any oxide spallation has been detected for this duration range. In the present study, the mass gain after 500 hours seems to diverge from the initial parabolic curve (dashed curves in Fig. 2), reflecting a breakaway regime. Despite such a change in kinetics at high temperature for extended oxidation durations, these results suggest a better oxidation resistance when Zr is added simultaneously with Mo and Si in the alloy. Their relative contents were sufficient to avoid the formation of Ti<sub>5</sub>Si<sub>3</sub> [20], SiO<sub>2</sub> [18] and ZrO<sub>2</sub> [21].

XRD analyses coupled with EPMA maps show that two different oxidation temperatures used for long-term oxidation experiments, 700 and 800 °C, lead to the formation of multi-layered oxide with alternating TiO<sub>2</sub> and AlNbO<sub>4</sub> layers. This result is in agreement with other studies carried out on Ti-Al-Nb alloys containing O-phase [14,15,29]. Compared to Ti-Al alloys containing less than 10 at. % of Nb [25,28,30], Al<sub>2</sub>O<sub>3</sub> was not detected by XRD in this work. The formation of Al<sub>2</sub>O<sub>3</sub> should be prohibited by the Nb content higher than 10 at. %, which favors the formation of Nb-rich oxides such as AlNbO<sub>4</sub> as it was observed by Yoshihara et al. [13].

#### 4.2. Long-term oxidation behaviour

The oxide has a multilayer structure, as already observed for other Ti-Al base alloys [15,28,31]. According to XRD and EPMA analyses, the oxide consists of alternating TiO<sub>2</sub> and AlNbO<sub>4</sub> layers and the structure of this multilayer oxide scale does not depend on temperature and oxidation time. This is also in agreement with results obtained by Leyens [14] for Ti-22Al-25Nb alloy after oxidation in dry and humid air between 650 and 1100 °C. On the contrary, Ti-22Al-26Nb-6Zr (at.%) alloy exhibits a chemical evolution of the oxide scale with temperature, where the ZrO<sub>2</sub> oxide is formed at 800 °C after 100 h of oxidation [32]. This could be attributed to the higher content of Zr (6 at.%) in the alloy promoting ZrO<sub>2</sub> formation.

A thin N-rich layer, located close to the oxide/alloy interface was observed after oxidation at 700 °C for 2000 and 5000 hours and at 800 °C for 1506 hours. According to several studies, this thin N-rich layer could consist of TiN [25], NbN [11] or a mixed (Ti,Nb,Al)N compounds [15].

The oxygen enrichment of the alloy during oxidation in lab air was observed for all conditions. It results in the formation of the  $\alpha$ -case layer [33], which could have a detrimental effect on mechanical properties such as ductility and, especially, fatigue strength, due to increased hardness and brittleness of the subsurface. As reported in literature [28,34], the thickness of the  $\alpha$ -case layer increases with temperature and oxidation time. Nevertheless, the measured thickness of the  $\alpha$ -case layer for the present advanced Ti<sub>2</sub>AlNb alloy is less than that obtained for Ti-64 and Ti-6242 alloys oxidized at 700 °C for hours (200 and 108  $\mu$ m respectively) [26].

Oxygen enrichment of the alloy close to the oxide/alloy interface was evidenced by EPMA (Figs. 4,5 and 9). Effective diffusion coefficient for oxygen in the alloy can be estimated using the classical solution of the Fick's second equation for the constant diffusion source and semi-infinite substrate configuration, according to the Eq. (2):

$$C(x, t) = A + B \operatorname{erf}\left(\frac{x}{2\sqrt{Dt}}\right) \quad (2)$$

where  $C(x,t)$  is the concentration of oxygen,  $x$  is the penetration depth,  $t$  is the time,  $D$  is the effective oxygen diffusion coefficient and  $A$  and  $B$  constants depending on initial and limit conditions. The values of  $D$  can be obtained from experimental oxygen concentration profiles by fitting Eq. (2) (Figs. 7a and c and Fig. 11a). It is worth noting that the measured concentration profiles are characterized by (i) first rapid initial drop in oxygen content as function of distance followed by (ii) region with a progressive decrease in oxygen content and (iii) base alloy region where initial oxygen concentration was not significantly affected by oxygen diffusion. Moreover, the first region is characterized by increased oxygen concentration that was found to be higher than oxygen solubility limit in the alloy. It is supposed thus that this region contained a mixture of different oxides and metallic matrix. The first region should contain as well several nitrides as mentioned earlier since the N-rich layer was observed there (Figs. 4,5 and 9) and the N content was increased in comparison with that measured in the region (ii). Therefore, only the data obtained in the second region with a progressive decrease in oxygen content were used for the diffusion coefficient estimation.

Considering that the alloy surface enrichment by oxygen leads to hardening, Leyens [14] and Ralison et al. [15] were able to estimate oxygen diffusion coefficients from microhardness measurements, assuming that the oxygen concentration is proportional to the hardness value. Therefore, microhardness data obtained in the present work were used as well to estimate oxygen diffusion coefficients using Eq. (2) substituting the oxygen concentration by hardness (Figs. 7b and d and Fig. 11a). One can see that Eq. (2) describes well the concentration and microhardness profiles (Figs. 7b and d). The obtained diffusion coefficients are summarized in Table 4. It is worth noting that a good agreement is observed between the results obtained from concentration profiles and microhardness.

When compared to the literature data, the effective oxygen diffusion coefficients for the present alloy obtained by hardness measurements are 3-4 orders of magnitude smaller than those estimated by Sefer for Ti-64 and Ti-6242 alloys oxidized at 700 °C for 500 hours ( $2.10^{-14}$  and  $5.10^{-15}$   $\text{m}^2.\text{s}^{-1}$ , respectively) [26]. Such a decrease in oxygen diffusion should explain the reduction of  $\alpha$ -case thickness observed in this study in comparison with that in Ti64 and Ti6242. Moreover, the effective oxygen diffusion coefficients at 800 °C show the beneficial effect of Zr, Si and Mo additions for reducing oxygen diffusion, since the obtained value ( $\sim 10^{-16}$   $\text{m}^2.\text{s}^{-1}$ ) is one order of magnitude smaller than that measured by Leyens [14] for Ti-22Al-25Nb at 800 °C ( $10^{-15}$   $\text{m}^2.\text{s}^{-1}$ ). Ralison et al. [15] measured diffusion coefficient values of  $1.2.10^{-16}$   $\text{m}^2.\text{s}^{-1}$  for a Mo- and Si-containing Ti-23Al-25Nb-1Mo-0.25Si alloy oxidized at 650 °C, suggesting once more the beneficial effect of simultaneous addition of Mo, Si and Zr.

**Table 4.** Oxygen effective diffusion coefficient ( $\text{m}^2 \text{s}^{-1}$ ) obtained from oxygen concentration profiles and microhardness measurements after oxidation at 700 and 800 °C for different durations

Method	Oxidation time (hours)		
	700 °C		800 °C
	2000	5000	1506
Oxygen profile (EDS)	$2.9.10^{-17}$	$1.7.10^{-17}$	$2.0.10^{-16}$
Microhardness measurements	$6.7.10^{-17}$	$4.8.10^{-17}$	$1.2.10^{-16}$

### 4.3. Oxidation mechanism

As illustrated in Figs. 8 and 13, remnants of substrate microstructure (precipitates of O-phase and grain boundaries) are visible in the oxide scale. The same observation was done for a Ti-23Al-13Nb-5Ta-3Mo alloy oxidized for 300 h at 800 °C in synthetic air [15]. According to several studies on Nb-base alloys [35-37], these observations confirm the fact that the oxide scale growth is driven by inward diffusion of oxygen.

Using the observations done in this work, an oxidation mechanism can be proposed at 700 and 800 °C (Fig. 14): (1) Oxygen diffuses into the base alloy by an inward mechanism. Titanium begins to react with oxygen atoms to form rutile ( $\text{TiO}_2$ ) whereas aluminium and niobium react to form aluminium niobate ( $\text{AlNbO}_4$ ). Both oxides grow by alternating layers to produce the multi-layered structure. (2) A N-rich layer is formed and grown with the oxidation duration. The oxide layer continues to grow by an inward mechanism, consuming the  $\alpha$ -case layer formed previously. Oxygen is still diffusing in the substrate however the growth of oxide and N-rich layers decreases the oxygen flux.

As observed previously, the thickness of the N-rich layer, located at the interface between the oxide and the  $\alpha$ -case layer, increases with the oxidation duration and temperature. Leyens supposed that the nitrogen was still diffusing with oxygen through the oxide layer [14]. Nevertheless, the appearance and growth of the N-rich layer could also be due as well to a nitrogen drag present in the  $\alpha$ -case layer by oxide/substrate interface.

## 5. CONCLUSIONS

The oxidation behaviour of an advanced Ti<sub>2</sub>AlNb alloy was investigated over a temperature range of 650-800 °C in lab air for short- and long-term experiments. The main results can be summarized as follows:

- The mass gain increased with time and temperature and oxidation kinetics was parabolic at 650 and 700 °C for durations up to 1000 hours, while the parabolic oxidation rate was changed at 800 °C between 500 and 1000 hours.
- The long-term oxidation experiments (at 700 °C for 2000 and 5000 hours and at 800 °C for 1506 hours) revealed the same multilayer oxide scale formation consisting of alternating  $\text{TiO}_2$  and  $\text{AlNbO}_4$ .
- The formation of N-rich layer was observed at oxide/alloy interface for each oxidized sample.
- Thickness of the  $\alpha$ -case layer increase with the temperature and duration of oxidation
- Oxide layers grow by inward oxygen diffusion.
- Comparison with the literature data revealed that the oxidation resistance of the used Ti<sub>2</sub>AlNb alloy is better than that in conventional  $\alpha+\beta$  titanium alloys (as Ti-64, Ti-6242 and IMI 834) with lower parabolic rate constant  $k_p$  and smaller  $\alpha$ -case layer thickness.
- Additions of Mo, Zr and Si alloying elements improve the oxidation resistance of Ti<sub>2</sub>AlNb alloys without formation of brittle phases.
- Oxygen diffusion in the studied alloy was found to be slower than in other titanium base alloys resulting as well in improved oxidation resistance.

### Acknowledgements

The authors would like to acknowledge Karim Inal and Gabriel Monge (Centre de Mise en Forme des Matériaux, MINES ParisTech) for the XRD measurements and Lynh-Thy Tran-Hoang (Centre des

Matériaux, MINES ParisTech) for the EPMA analyses. This study was supported by the program “Cristal” funded by Safran Tech and Centre des Matériaux.

## References

1. F.H. Froes, C. Suryanarayana, Titanium aluminides, N.S. Stoloff, V.K. Sikka (eds.), Physical metallurgy and processing of intermetallic compounds (Chapman & Hall, New York, 1996) 297-350.
2. J. Kumpfert, C. Leyens, Orthorhombic titanium aluminides: Intermetallics with improved damage tolerance, C. Leyens, M. Peters (eds.), Titanium and titanium alloys: Fundamentals and applications (Wiley-VCH, Weinheim, 2003) 59-88.
3. W. Chen, J.W. Li, L. Xu, B. Lu, Development of Ti<sub>2</sub>AlNb alloys: Opportunities and challenges, Ad. Mater. Process. 172 (2014) 23-27.
4. A. Gil, E. Wallura, H. Grübmeier, W.J. Quadackers, The influence of cooling rate during alloy casting on the oxidation behavior of TiAl-based intermetallics, J. Mater. Sci. 28 (1993) 5869-5874.
5. I.E. Locci, M.P. Brady, J.L. Smialek, Long term oxidation of model and engineering TiAl alloys, Mater. Res. Soc. Symp. Proc. 646 (2001) 1-6.
6. S. Tkachenko, O. Datskevich, K. Dvořák, Z. Spetz, L. Kulak, L. Čelko, Isothermal oxidation behavior of experimental Ti-Al-Si alloys at 700°C in air, J. Alloy. Compd 694 (2017) 1098-1108.
7. C. Wagner, Reaktionstypen bei der oxydation von legierungen, Z. Elektrochem. 63 (1959) 772-782.
8. J.P. Lin, L.L. Zhao, G.Y. Li, L.Q. Zhang, X.P. Song, F. Ye, G.L. Chen, Effect of Nb on oxidation behavior of high Nb containing TiAl alloys, Intermetallics 19 (2011) 131-136.
9. A.K. Gogia, T.K. Nandy, D. Banerjee, T. Carisey, J.L. Strudel, J.M. Franchet, Microstructure and mechanical properties of orthorhombic alloys in the Ti-Al-Nb system, Intermetallics 6 (1998) 741-748.
10. L. Germann, D. Banerjee, J.Y. Guédou, J.L. Strudel, Effect of composition on the mechanical properties of newly developed Ti<sub>2</sub>AlNb-based titanium aluminide, Intermetallics 13 (2005) 920-924.
11. J.H. Kim, S. Emura, Y.T. Lee, High temperature oxidation behavior of Ti<sub>2</sub>AlNb intermetallic alloys, Int. J. Metall. Mater. Eng. 1 (2015) 1-6.
12. D. Banerjee, A.K. Gogia, T.K. Nandi, V.A. Joshi, A new ordered orthorhombic phase in a Ti<sub>3</sub>Al-Nb alloy, Acta Metall. 36 (1988) 871-882.
13. M. Yoshihara, K. Miura, Effects of Nb addition on oxidation behavior of TiAl, Intermetallics 3 (1995) 357-363.
14. C. Leyens, Environmental effects on orthorhombic alloy Ti-22Al-25Nb in air between 650 and 1000°C, Oxid. Met. 52 (1999) 475-503.
15. A. Ralison, F. Dettenwanger, M. Schütze, Oxidation of orthorhombic Ti<sub>2</sub>AlNb alloys in the temperature range 550-1000°C in air, Mater. High Temp. 20 (2003) 607-629.
16. L. Gauer, S. Alpérine, P. Steinmetz, A. Vassel, Influence of niobium additions on high-temperature oxidation behavior of Ti<sub>3</sub>Al alloys and coatings, Oxid. Met. 42 (1994) 49-74.
17. L. Kong, J. Qi, B. Lu, R. Yang, X. Cui, T. Li, T. Xiong, Oxidation resistance of TiAl<sub>3</sub>-Al composite coating on orthorhombic Ti<sub>2</sub>AlNb based alloy, Surf. Coat. Technol. 204 (2010) 2262-2267.
18. Y. Shida, H. Anada, Role of W, Mo, Nb and Si on oxidation of TiAl in air at high temperatures, Mater. Trans. 35 (1994) 623-631.
19. Y. Shida, H. Anada, The effect of various ternary additives on the oxidation behavior of TiAl in high-temperature air, Oxid. Met. 45 (1996) 197-219.
20. H.R. Jiang, Z.L. Wang, W.S. Ma, X.R. Feng, Z.Q. Dong, L. Zhang, Y. Liu, Effects of Nb and Si on high temperature oxidation of TiAl, Trans. Nonferrous Met. Soc. China 18 (2008) 512-517.
21. W. Dang, J.S. Li, T.B. Zhang, H.C. Kou, Oxidation behavior of Zr-containing Ti<sub>2</sub>AlNb-based alloy at 800°C, Trans. Nonferrous Met. Soc. China 25 (2015) 783-790.
22. J.Y. Guédou, J.M. Franchet, J.L. Strudel, L. Germann, D. Banerjee, V. Kumar, T. Nandy, E. Laik, Patent WO 2016102806 A1 (2016).
23. K. Muraleedharan, T.K. Nandy, D. Banerjee, S. Lele, Phase stability and ordering behavior of the O phase in Ti-Al-Nb alloys, Intermetallics 3 (1995) 187-199.
24. D. Monceau, B. Pieraggi, Determination of parabolic rate constants from a local analysis of mass-gain curves, Oxid. Met. 50 (1998) 477-493.

25. S.Y. Park, D.Y. Seo, S.W. Kim, S.E. Kim, J.K. Hong, D.B. Lee, High temperature oxidation of Ti-46Al-6Nb-0.5W-0.5Cr-0.3Si-0.1C alloy, *Intermetallics* 74 (2016) 8-14.
26. B. Sefer, *Oxidation and alpha-case phenomena in titanium alloys used in aerospace industry: Ti-6Al-2Sn-4Zr-2Mo and Ti-6Al-4V* (PhD thesis, Lulea University of Technology, 2014).
27. S. Becker, A. Rahmel, M. Schorr, M. Schütze, Mechanism of isothermal oxidation of the intermetallic TiAl and of TiAl alloys, *Oxid. Met.* 38 (1992) 425-464.
28. H. Guleryuz, H. Cimenoglu, Oxidation of Ti-6Al-4V alloy, *J. Alloys Compd* 472 (2009) 241-246.
29. C. Roos, D. Oquab, B. Pieraggi, High temperature oxidation of Nb-Ti-AL alloys, *Mater. Sci. Forum* 251-254 (1997) 119-126.
30. I.E. Locci, M.P. Brady, R.A. MacKay, J.W. Smith, Very long term oxidation of Ti-48Al-2Cr-2Nb at 704°C in air, *Scripta Mater.* 37 (1997) 761-766.
31. J. Dai, J. Zhu, C. Chen, F. Weng, High temperature oxidation behavior and research status of modifications on improving high temperature oxidation resistance of titanium alloys and titanium aluminides: a review, *J. Alloys Compd* 685 (2016) 784-798.
32. W. Dang, J.S. Li, T. Zhang, H.C. Kou, High-temperature oxidation behavior of Ti-22Al-27(Nb, Zr) alloys, *Rare Metal Mater. Eng.* 44 (2015) 261-266.
33. R.R. Boyer, An overview on the use of titanium in the aerospace industry, *Mater. Sci. Eng. A* 213 (1996) 103-114.
34. A.M. Bauristhene, K. Mutombo, W.E. Stumpf, Alpha case formation mechanism in Ti-6Al-4V alloy investment castings using YFSZ shell moulds, *J. South. Afr. Inst. Min. Metall.* 113 (2013) 357-361.
35. J. Geng, P. Tsakirooulos, G. Shao, A thermo-gravimetric and microstructural study of the oxidation of Nb<sub>85</sub>/Nb<sub>5</sub>Si<sub>3</sub>-based *in situ* composites with Sn addition, *Intermetallics* 15 (2007) 270-281.
36. J. Wang, X.P. Guo, J.M. Guo, Effects of B on the microstructure and oxidation resistance of Nb-Ti-Si-based ultrahigh-temperature alloy, *Chinese Journal of Aeronautics* 22 (2009) 544-550.
37. S. Mathieu, S. Knittel, P. Berthod, S. Mathieu, M. Vilasi, On the oxidation mechanism of niobium-base *in situ* composites, *Corr. Sci.* 60 (2012) 181-192.

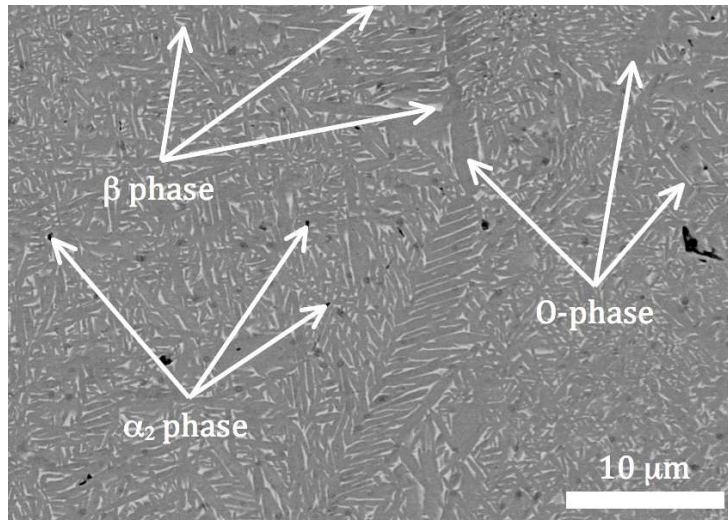


Fig. 1. Final microstructure of the studied alloy after elaboration.

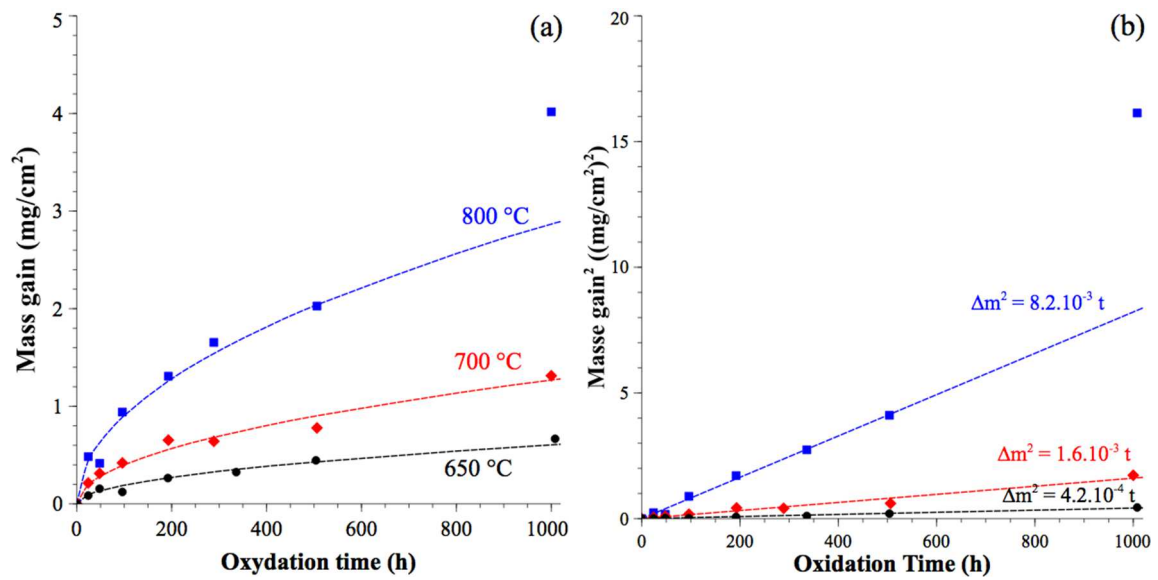


Fig. 2. Oxidation of the studied alloy at 650, 700 and 800 °C: (a) Evolution of mass gain with oxidation time; (b) Linearization of square of mass gain vs. time. The dashed lines correspond to the fit using the Eq. (1).

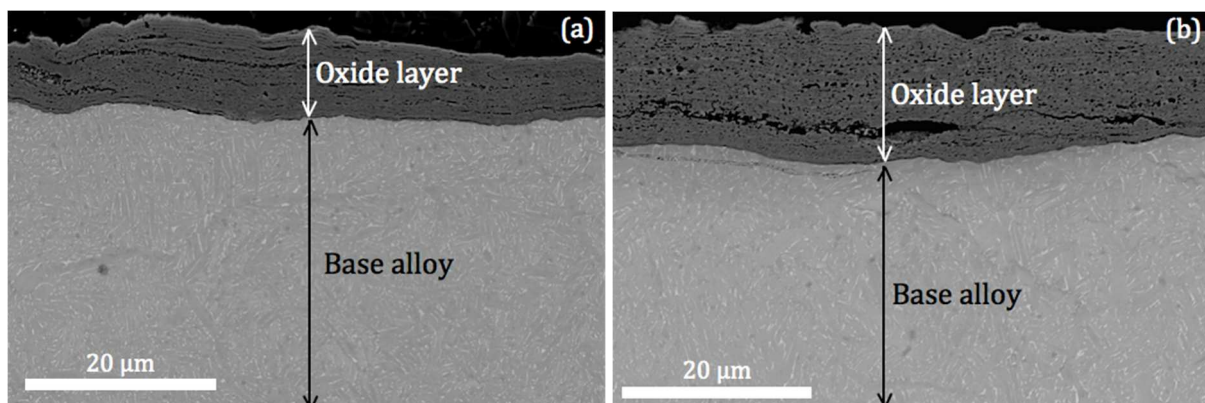
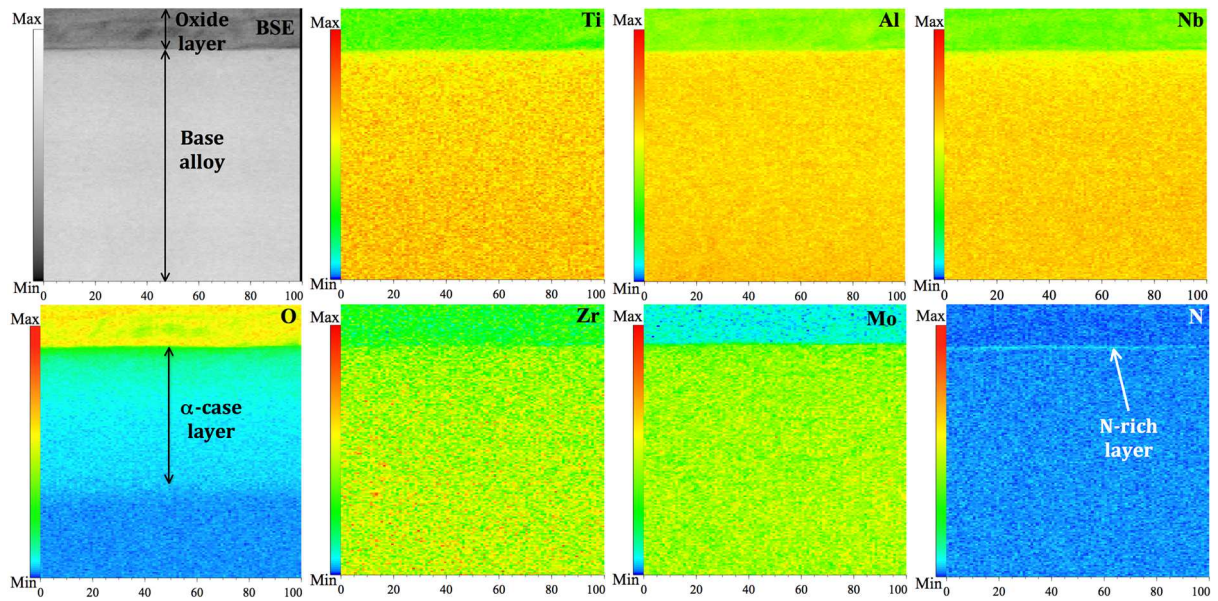
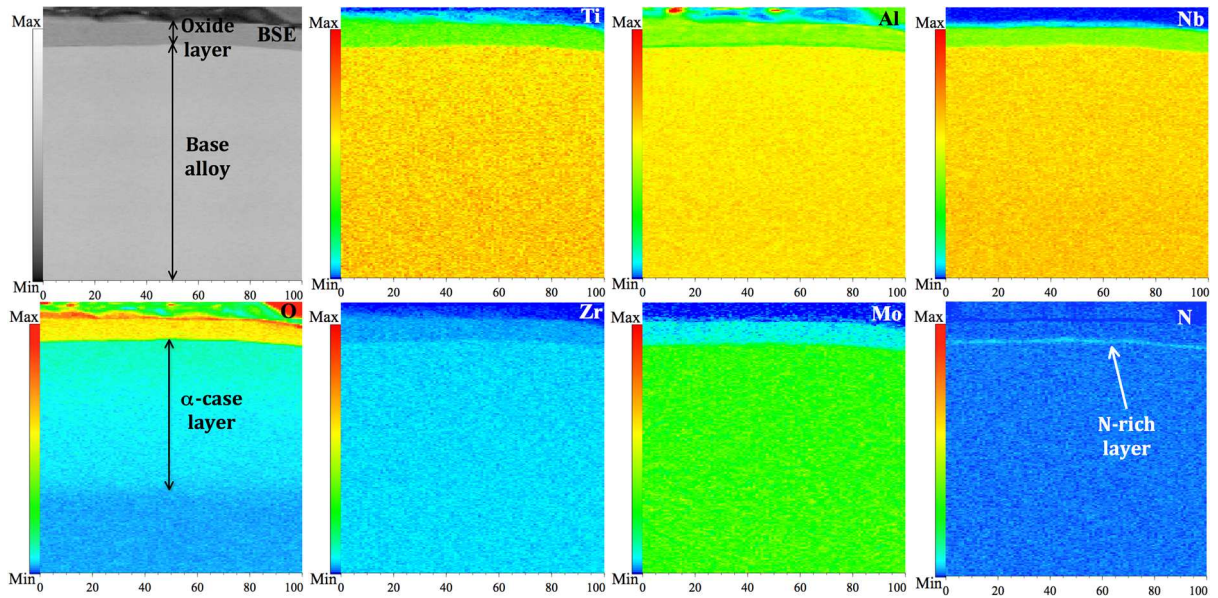


Fig. 3. Microstructure of the studied alloy close to the alloy/oxide interface observed after oxidation at 700 °C for (a) 2000 hours and (b) 5000 hours (SEM/BSE).



**Fig. 4.** BSE and corresponding EPMA maps for different elements after oxidation at 700 °C for 2000 hours. Y- and X-axis correspond to a distance in  $\mu\text{m}$ .



**Fig. 5.** BSE and corresponding EPMA maps for different elements after oxidation at 700 °C for 5000 hours. Y- and X-axis correspond to a distance in  $\mu\text{m}$ .

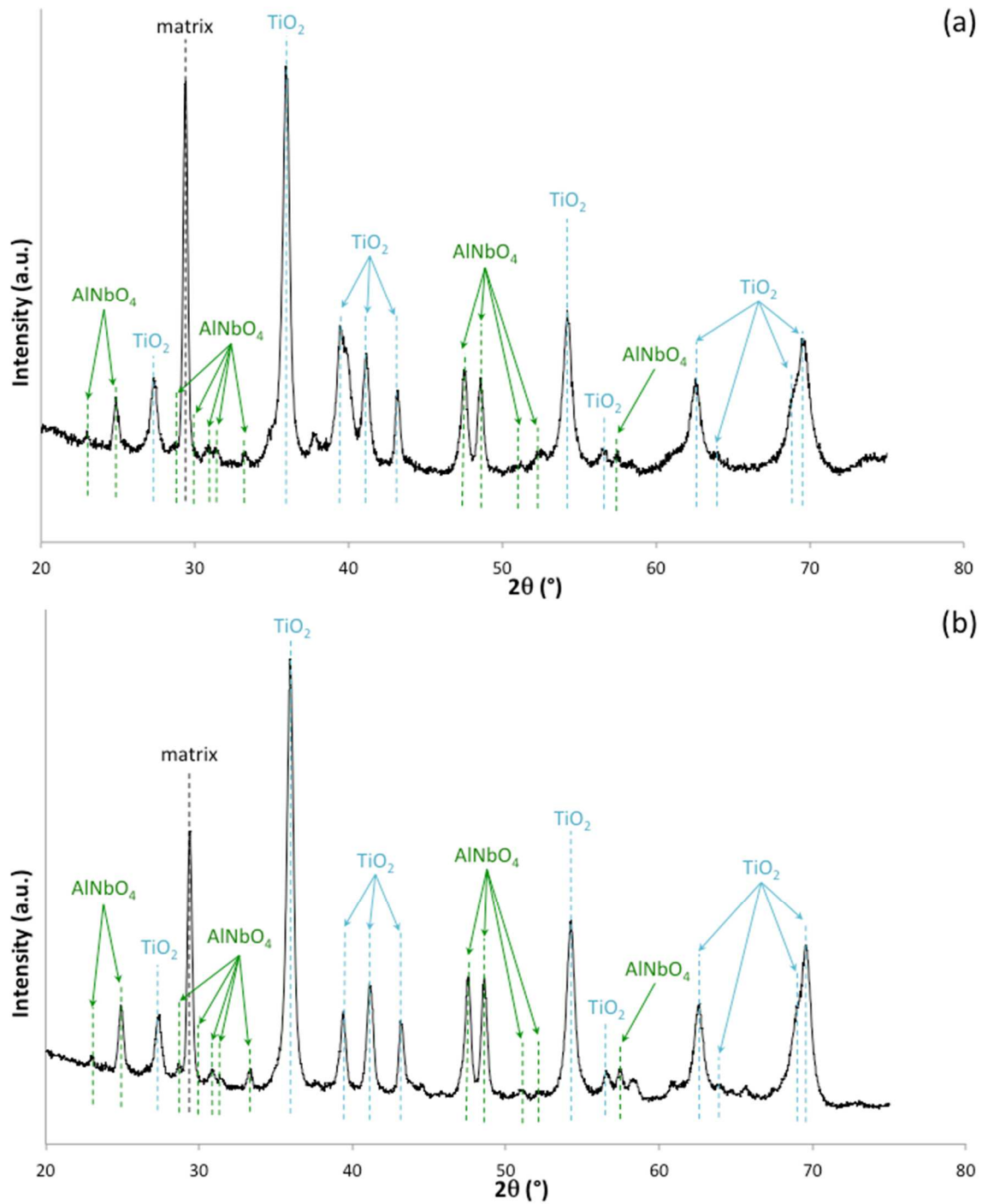


Fig. 6. XRD patterns after oxidation at 700 °C for (a) 2000 and (b) 5000 hours.

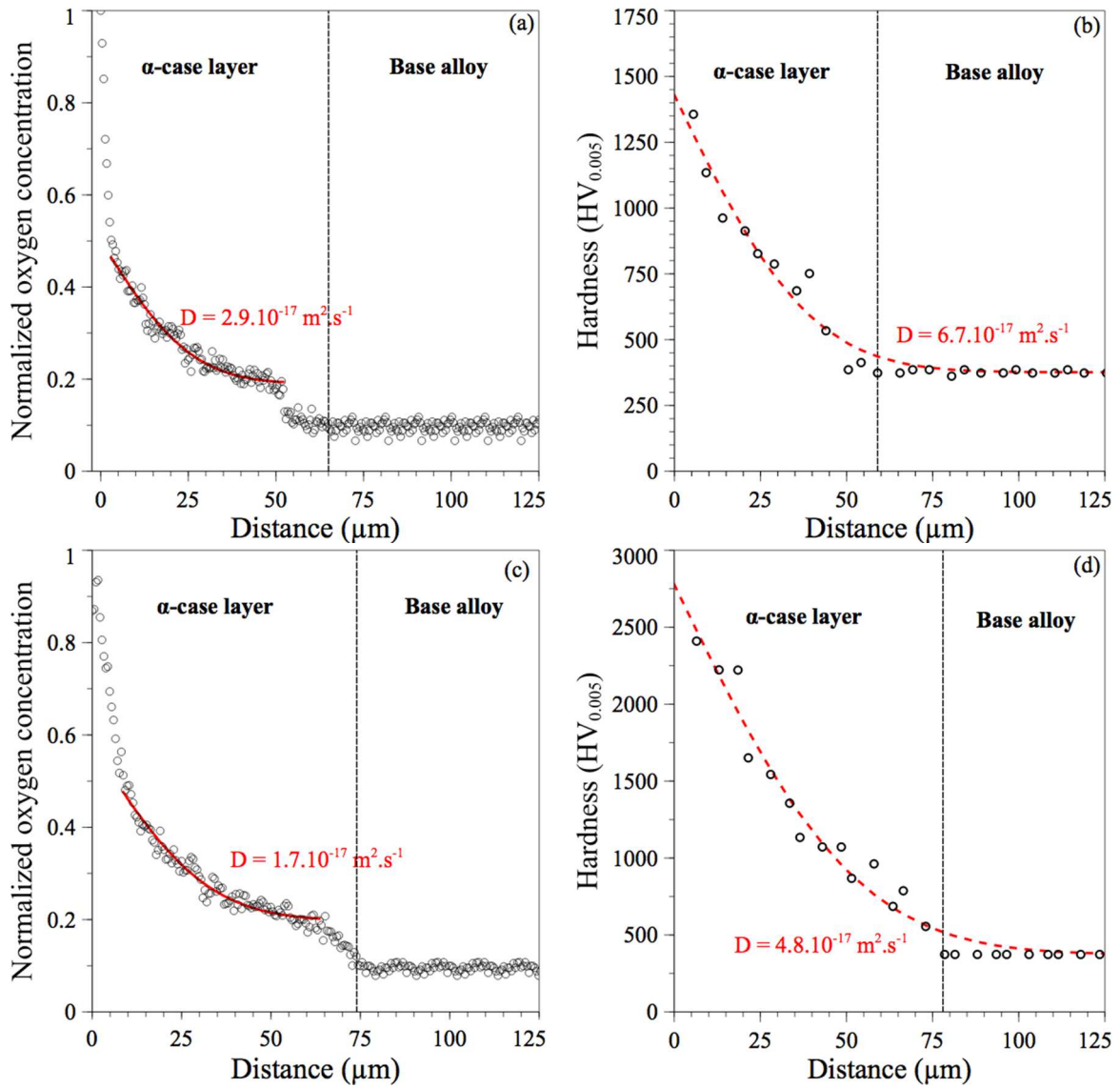


Fig. 7. Oxygen concentration profiles and corresponding microhardness values from the interface oxide/alloy (Distance=0) to the base alloy after oxidation at 700 °C for (a) and (b) 2000 hours and (c) and (d) 5000 hours. The red lines correspond to the fit of the data by Eq. (2).

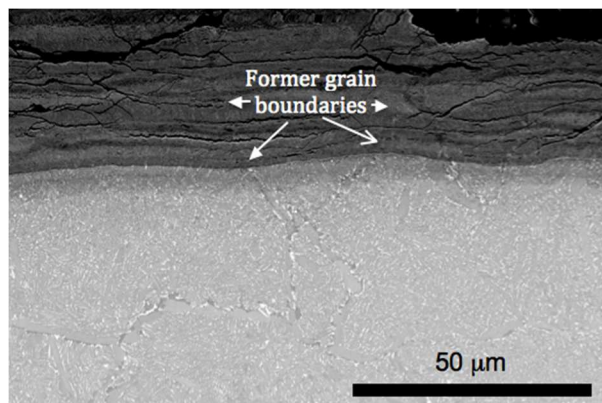
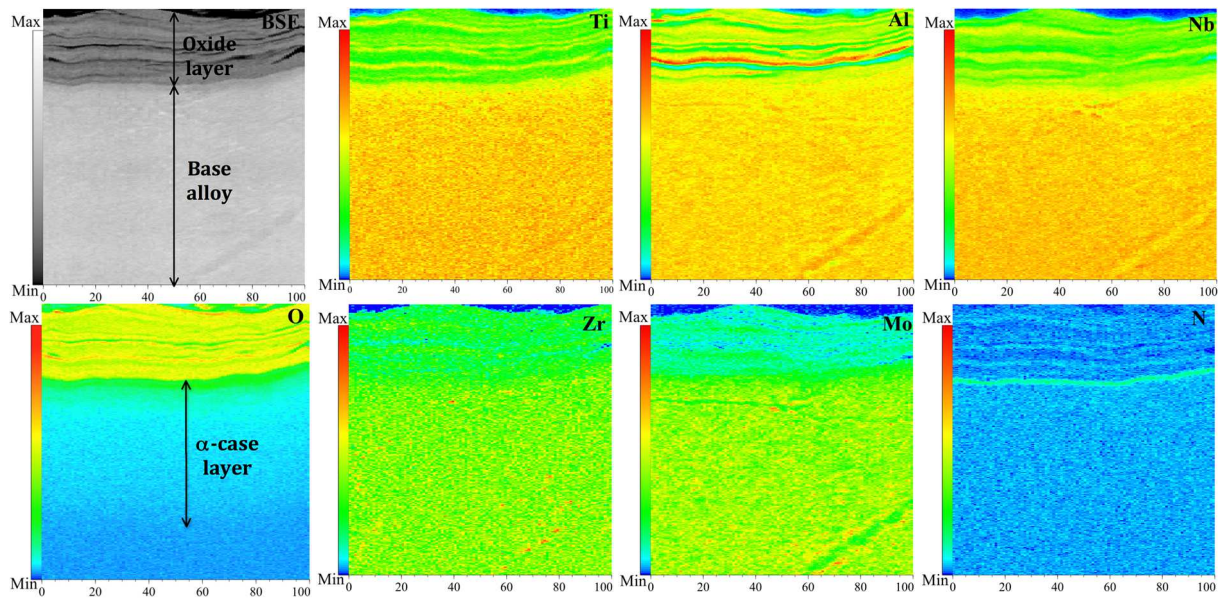
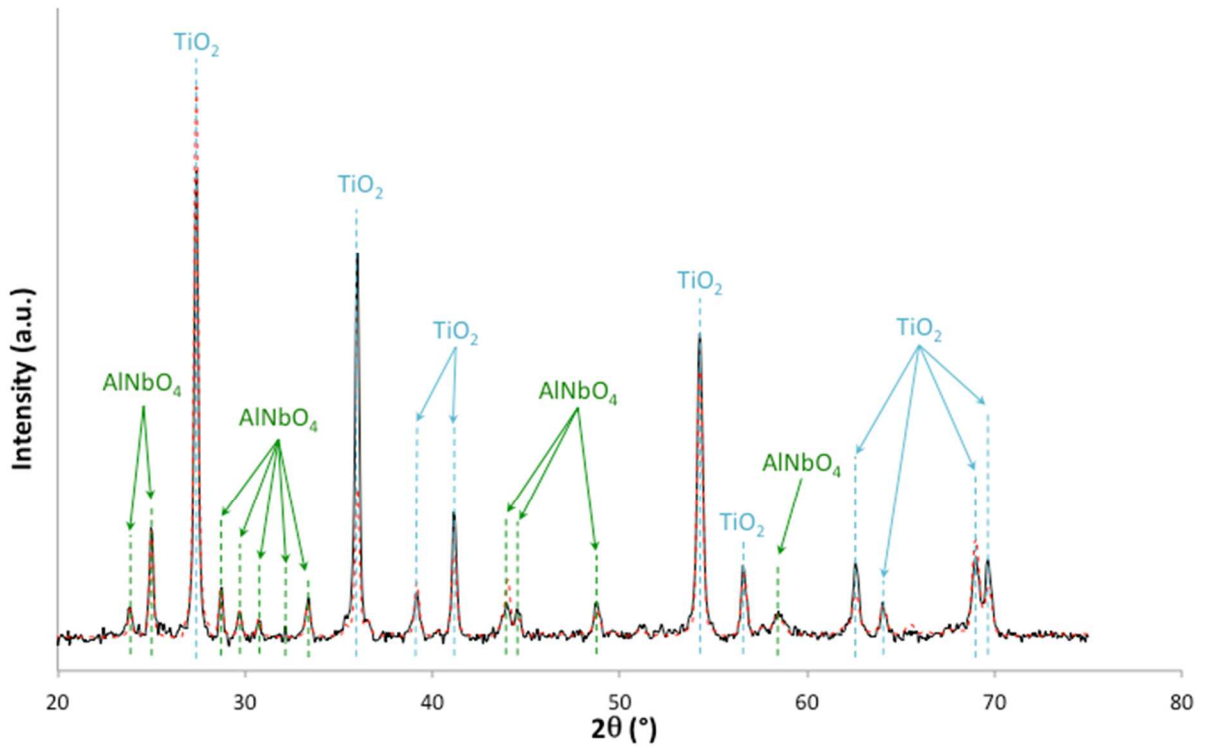


Fig. 8. Microstructure of the studied alloy close to alloy/oxide interface observed after oxidation at 800 °C for 1506 hours (SEM/BSE).



**Fig. 9.** BSE and corresponding EPMA maps for different elements after oxidation at 800 °C for 1506 hours. Y- and X-axis correspond to a distance in  $\mu\text{m}$ .



**Fig. 10.** Rietveld refinement (red dashed) of XRD pattern (black solid) after oxidation at 800 °C during 1506 hours.

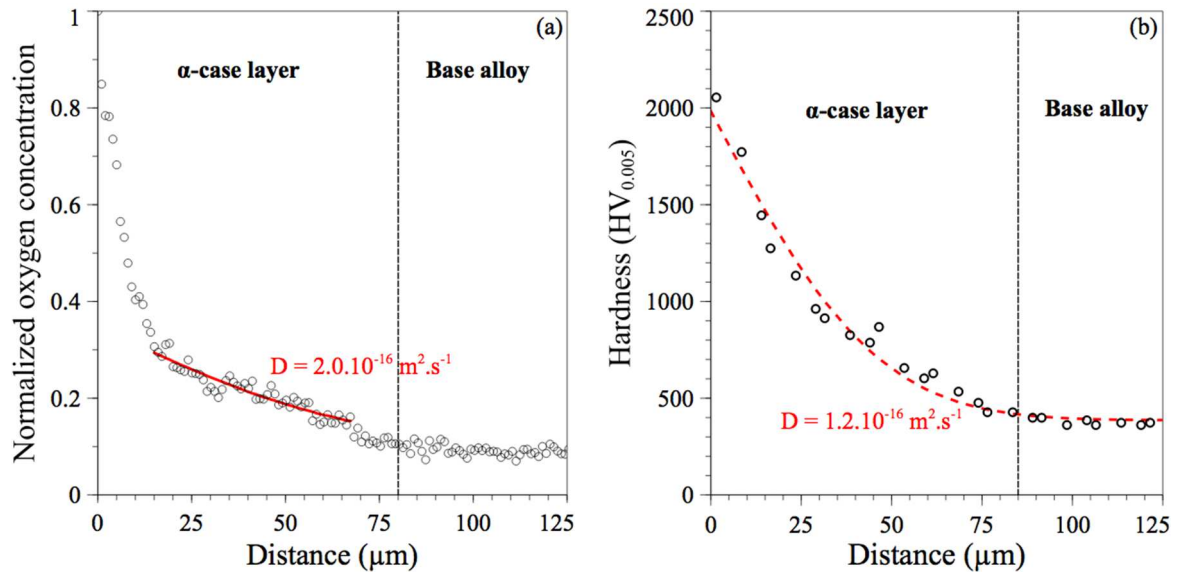


**Fig. 11.** Analysis of the  $\alpha$ -case layer after oxidation at 800 °C for 1506 hours using (a) Oxygen concentration profile measured by EDS and (b) microhardness measurements from the interface oxide/alloy (Distance=0) to the base alloy. The red lines correspond to the fit of the curves by Eq. (2).

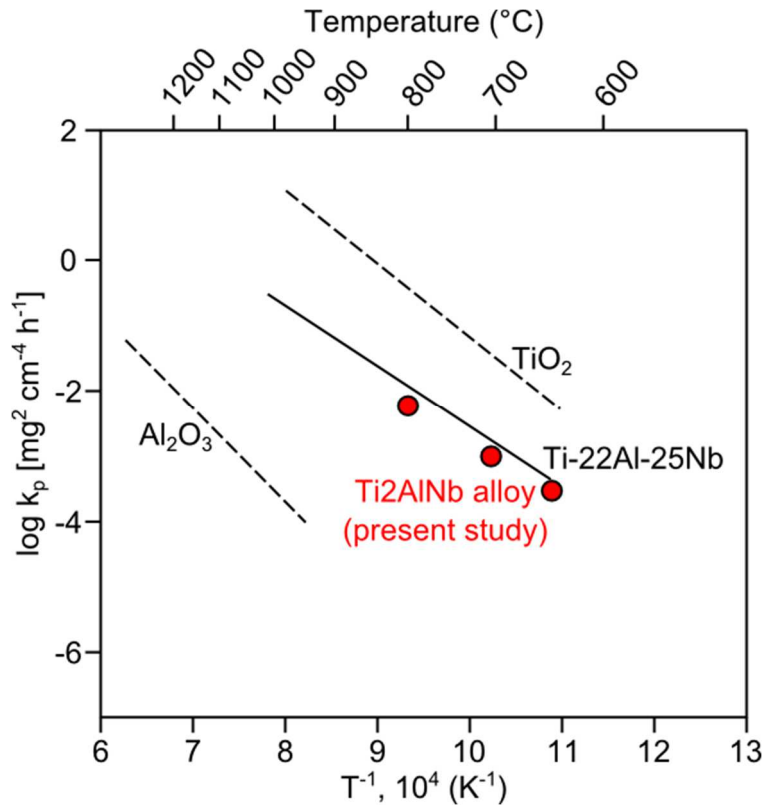


**Fig. 12.** Temperature dependence for the parabolic rate constant  $k_p$  for the studied alloy used in the present study (red circles) compared with literature data for Ti-22Al-25Nb alloy [14]. The  $\text{TiO}_2$  dashed line represents the oxidation kinetics for pure titanium, whereas the  $\text{Al}_2\text{O}_3$  dashed line was obtained for TiAl oxidation.

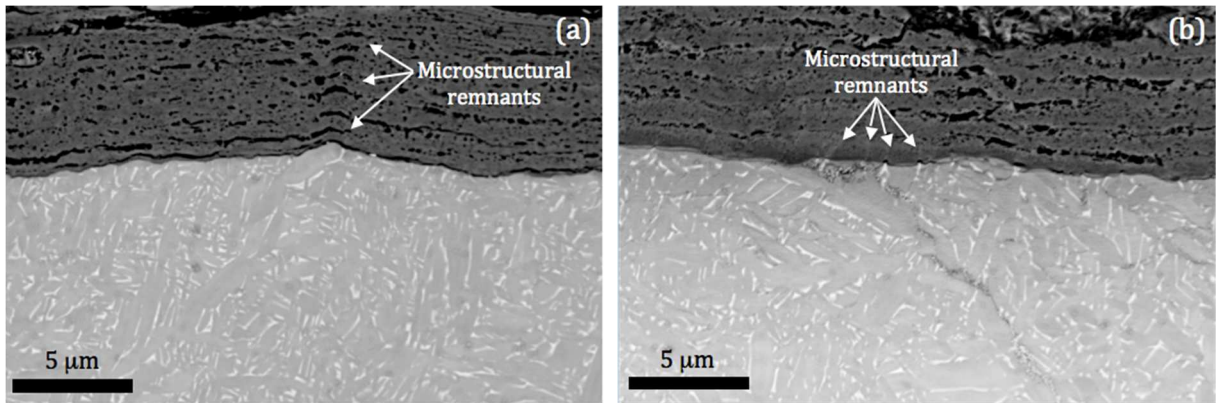


**Fig. 13.**  $\alpha$ -case layer microstructure close to the alloy/oxide interface after oxidation at 700 °C for (a) 2000 hours and (b) 5000 hours. The oxide layer is on the top of the pictures whereas the  $\alpha$ -case layer is on the bottom.

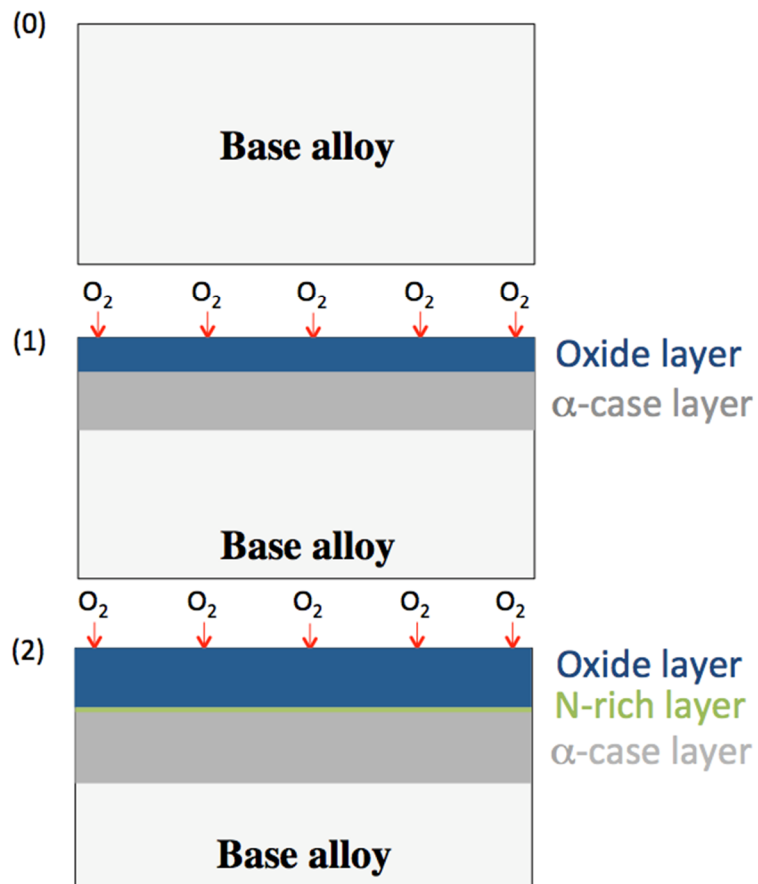


**Fig. 14.** Schematic representation of oxidation mechanism at 700 and 800 °C.

